Simulation of LSD Wave Characteristics in Ar and N_2 Using a 1-D Laser-induced Discharge Model Coupled with Hydrodynamic Relations for Laser-propelled Thruster Studies

IEPC-2015-175／ISTS-2015-b-175

Presented at Joint Conference of 30th International Symposium on Space Technology and Science 34th International Electric Propulsion Conference and 6th Nano-satellite Symposium, Hyogo-Kobe, Japan July 4 – 10, 2015

Joseph A. Ofosu[1]
The University of Tokyo, Kashiwa, Chiba, 277-8561, Japan

Kohei Matsui[2] and Kimiya Komurasaki[3]
The University of Tokyo, Bunkyo-ku, Tokyo, 113-8656, Japan

Kohei Shimamura[4]
The University of Tsukuba, Tsukuba, Ibaraki, 305-8573, Japan

and

Hiroyuki Koizumi[5]
The University of Tokyo, Kashiwa, Chiba, 277-8561, Japan

Abstract: Repetitively pulsed laser propulsion is one of the key beamed energy propulsion (BEP) candidate technology for future space missions. In order to achieve an efficient laser propelled thruster, it is vital to comprehend the Physics of laser-absorption and energy conversion processes of laser supported detonation (LSD) in a laser-produced plasma. In LSD waves, an absorption layer and shock front travel together in which energy is transferred efficiently from laser energy to kinetic energy. However, due to the decay in the intensity of a pulse-laser and the increasing beam cross sectional area of focusing optics, a separation in travel occurs leading to the termination of LSD and subsequent cessation of the transfer process. After the separation, the shock wave propagates adiabatically and inefficiently. It is therefore important to understand the LSD termination and its relation to ambient gas content especially for the outer atmosphere (rocket mode) application. We present in this paper, a comparison between measured and estimated ionization front velocities using a 1-D laser-induced discharge model and measured results.

[1] D.Sc. Candidate, Department of Advanced Energy, joseph@al.t.u-tokyo.ac.jp
[2] M.Eng. Candidate, Department of Aeronautics and Astronautics, k.matsui@al.t.u-tokyo.ac.jp
[3] Professor, Department of Aeronautics and Astronautics, komurasaki@k.u-tokyo.ac.jp
[4] Assistant Professor, Department Engineering Mechanics and Energy, shimamura@kz.tsukuba.ac.jp
[5] Associate Professor, Department of Advanced Energy, koizumi@al.t.u-tokyo.ac.jp

Nomenclature

A_{ik}	= transitional probability
c	= speed of light in vacuum
d	= width of test section or LSD
E_i	= excitation energy at level i
e	= electron charge magnitude
g_i	= statistical weight
h	= Planck constant/ number of fringe shifts
I_{ik}	= integrated line intensity
i_ν	= radiation due to free-free and free-bound transitions
K_n	= relative refractive index of neutral particle
k_B	= Boltzmann constant
M	= Mach number
m_e	= electron mass
N	= refractive index
n_e	= electron number density
n_j	= number density of species j
n_o	= number density of neutral particles outside plasma
q	= heat deposition
T_ex	= electron excitation temperature
U	= LSD wave velocity
U_R	= LSD wave velocity with electron-ion recombination effect
U_j	= internal partition function of species j
z	= displacement
α_R	= total recombination rate coefficient
γ	= ratio of specific heats
ε_o	= permittivity of free space
λ	= wavelength
λ_mfp	= mean free path of photon-absorption
ν_eff	= effective ionization frequency
ν_i	= ionization frequency
ϕ	= photon flux
Ω	= solid angle
Subscripts	
1	= 785 nm wavelength
2	= 470 nm wavelength
i	= upper energy level
k	= lower energy level

I. Introduction

LASER propulsion, a beamed energy propulsion (BEP) is one of the proposed transportation systems from ground to space. Its characteristic advantages are high specific impulse and high thrust as well as low propulsion weight since an on-board energy source is not required[1,2]. The original concept of propulsion by a beamed source such as a laser was proposed by Kantrowitz[3] and a typical application example is the Lightcraft by Myrabo[4]. Comparative cost reduction is one of the significant motivations for laser propulsion systems, as conventional chemical launch systems for space development projects are relatively expensive[5]. The successful development and implementation of this system is inseparable from the advances in high power lasers as well as socio-economic interests and investments.

The mechanism by which the beam source is absorbed to produce plasma in an ambient gas and to propagate an ionization wave efficiently for thrust generation is termed as laser supported detonation (LSD). In LSD waves, an absorption layer and shock front travel together in which energy is transferred efficiently from optical (laser) energy to kinetic energy. However, due to the decay in the intensity of a pulse-laser and the increasing beam cross sectional area of focusing optics, a separation in travel occurs leading to the termination of LSD and subsequent cessation of the transfer process. After the separation, the shock wave propagates adiabatically. It is essential therefore to understand the LSD termination and its dependence on the ambient gas properties especially for the rocket mode, since an on-board propellant would be needed for repetitive propulsion.

The influences of the focusing f number[6], ambient pressure[7] and laser power density[8] on LSD termination were investigated by Mori. Ushio et al[9] investigated Raizer's[10] effect quantitatively by a line focused laser beam. In their study, the lateral expansion from the LSD region to the ambient air was reduced by mechanically restricting the wave expansion in quasi-1D space using a wedged nozzle. This geometric restriction halved the laser intensity threshold for LSD termination and exhibited a relatively faster velocity of the LSD wave in the quasi-1D confinement compared with the 2-D case. We are of the view that Raizer's[12] theory of detonation is inadequate to describe the phenomenon observed in laser produced plasmas. The theory is simply based on the conservation of mass, momentum and energy, and stipulates that detonation is shockwave induced. Our recent studies[11-13] show that plasma propagation is a radiative induced phenomenon and thus pre-ionization due to photoionization and absorption play a significant role. Thus discharge-based physics is required to explain the generation and propagation process of the plasma's constituent particles such as electrons.

The objective of this study was to profile the laser-absorption layer in argon (Ar) and nitrogen (N_2) within the LSD termination region; compare measured and estimated ionization front velocity profiles using obtained measurements and a 1-D laser-induced discharge (LID) model including the effect of electron-ion recombination. The two-wavelength Mach-Zehnder interferometry and optical emission spectroscopy were the diagnostics tools applied for the determination of n_e and T_ex respectively, in order to estimate UV photon flux emitted toward the wavefront.

II. Description of the Visualization Technique for the LSD Wave

This section describes the optical apparatus used for both the interferometric and spectroscopic setups.

A. Lasers and Focusing Optics

A transversely excited atmospheric (TEA) CO_2 pulse laser with nominal energy of 10 J was used to produce plasma for the experiments. A joule meter was used to measure the pulse energy before and after the experiments. This was to ensure that the shot-to-shot pulse energy deviations were kept below ±5% throughout experimentation. The laser beam was focused by an off-axis parabolic mirror which has a focal length of 150 mm and then through a Zinc-Selenide (Zn-Se) window of the test chamber. The chamber pressure was set at 1 atm.

A diode pumped solid-state (DPSS) blue laser (continuous wave (CW), 470 nm, 20 mW) and an infra-red diode laser (CW, 785 nm, 100 mW) were the probe beams for the Mach-Zehnder interferometric study. Images and spectra of the laser induced plasma were taken using two (ICCD) cameras namely; iStar (Andor Tech. Inc., resolution 1,024×1,024 pixels, minimum exposure time of 2 ns) and Ultra 8 (DRS Tech., resolution 520×520 pixels, exposure time of 10 ns).

B. Two-Wavelength Mach-Zehnder Interferometry and Optical Emission Spectroscopy Setups

The schematic diagram for the two-wavelength Mach-Zehnder interferometer is as shown in Fig. 1. The near-infrared reflector was used to combine both beams into a single path before travelling through the spatial filter. The temporal and spatial resolutions were 100 ns and 10 μm (for blue laser) and 12 μm (for infra-red laser) respectively. Two line filters with specifications: 470 nm ± 10 nm and 785 nm ± 2 nm were used to suppress the plasma emission.

The schematic of the optical emission spectroscopy setup is as shown in Fig. 2. The plasma irradiation was collected using two plano-convex cylindrical lenses of focal length 150 mm and 300 mm respectively. The optical signal was focused into a Czerny-Turner spectrometer (MS3504i, SOL Instruments) coupled with an ICCD camera (iStar, Andor Technology). 50 sets of data were taken per each experimental condition in order to ensure consistency and accuracy of results. The spectrometer shutter exposure time was 100 ns. A xenon lamp and a halogen lamp were used to calibrate the wavelength and sensitivity respectively.

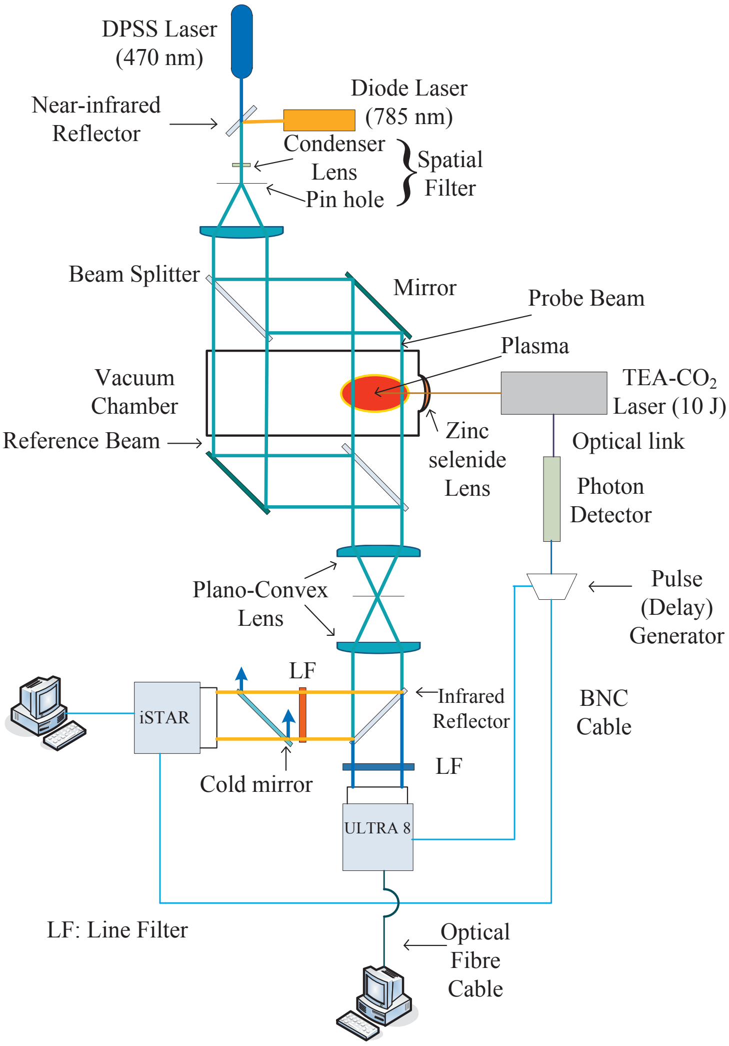

Figure 1. Schematic of Two-Wavelength Mach-Zehnder interferometer.

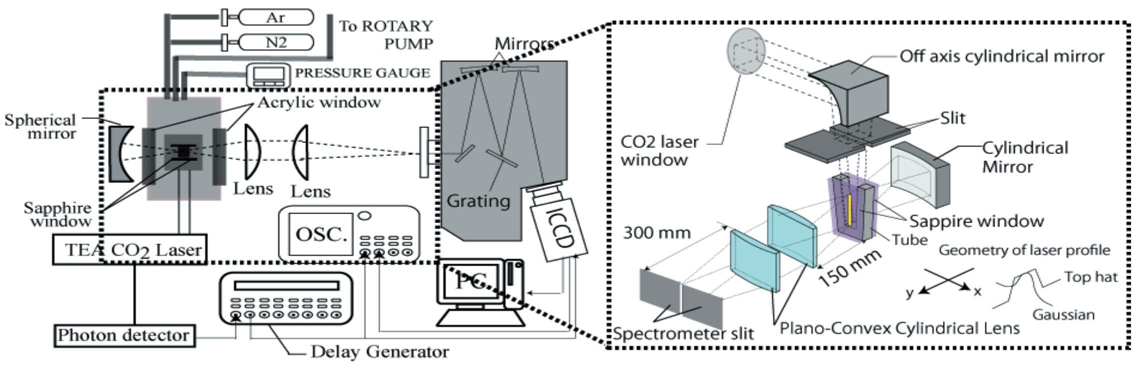

Figure 2. Schematic of Optical Emission Spectroscopy setup.

III. Determination of n_e, T_{ex} and LSD Wave Velocity Profiles

The electron number density n_e can be computed from measured refractive index distributions at two separate wavelengths (laser probe beams) as shown in Eq. (1). In order to obtain the change in refractive index ΔN in each probe beam, the fringe shifts h must be obtained.

$$n_e = \left(\frac{8\pi^2 c^2 m_e \varepsilon_o}{e^2}\right)\left(\frac{\Delta N_1 - \Delta N_2}{\lambda_1^2 - \lambda_2^2}\right). \tag{1}$$

h was deduced by analysing the intensity profile of the interference pattern along the axis of the interferogram. This was attained by comparing the shifted interference pattern with the reference (non-shifted) pattern. At the shock front, h was estimated using the normal shock relation and the relative refractive index of neutral particle K_n:

$$h = K_n n_o \left(\frac{(\gamma+1)M^2}{(\gamma-1)M^2+2} - 1\right)\frac{d}{\lambda}. \tag{2}$$

Where M, n_o, γ, and λ are the Mach number, number density of neutral particles outside plasma, ratio of specific heats and wavelength respectively. The thickness of the LSD wave phenomenon d was 2 mm.

The electron excitation temperature T_{ex} was evaluated from the Boltzmann plot equation (Eq. (3))[14], observed line spectra and physical parameters from NIST. These spectra were Ar II and N II lines observed in the range of 455 nm – 485 nm during the spectroscopic experiment and each taken at an elapsed time of 1.4 µs.

$$\ln\left(\frac{I_{ik}}{g_i A_{ik}}\right) = \ln\left(\frac{n_j}{U_j(T_{ex})}\right) - \frac{E_i}{k_B T_{ex}}. \tag{3}$$

Here A_{ik}, E_i, g_i, I_{ik}, k_B, n_j and U_j represent transitional probability, excitation energy, statistical weight, integrated line intensity, Boltzmann constant, number density of species j and the internal partition function of species j accordingly. Stark broadening was considered dominant because during the LSD regime, n_e is very high ($n_e \sim 10^{24}$ m^{-3}). Hence the obtained line spectra from experiment were fitted with the Lorentzian function.

Figures 3 (a) and (b) show the electron number density and excitation temperature distributions at an elapsed time of 1.4 µs respectively for Ar and N_2. Measured LSD wave velocity profiles versus laser intensity per unit density are shown in Fig. 5.

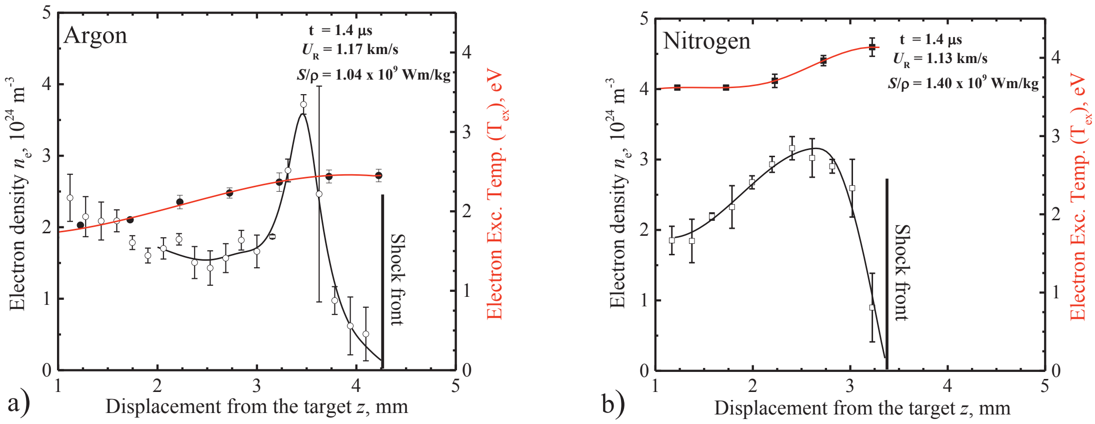

FIGURE 3. a) n_e and T_{ex} distributions in Ar. b) n_e and T_{ex} distributions in N_2.

The LSD termination times were 1.6 µs and 1.4 µs in Ar and N_2 accordingly. n_e is expected to be similar considering the formation of doubly ionized Ar ions, whiles N_2 would dissociate before ionization in most cases. At a given intensity, the energies required to achieve Ar^{++} (~43 eV) and N^+ (~40 eV) are almost similar, and the probable ionization process are as shown below in the reaction equation.

$$\left.\begin{array}{r}\mathrm{Ar}+e^{-}\rightarrow\mathrm{Ar}^{+}+2e^{-}\\ \mathrm{Ar}^{+}+e^{-}\rightarrow\mathrm{Ar}^{++}+2e^{-}\end{array}\right\},n_{\mathrm{e}}\sim 4e^{-}$$

$$\left.\begin{array}{r}\mathrm{N}_2\rightarrow 2\mathrm{N}\\ 2\mathrm{N}+2e^{-}\rightarrow 2\mathrm{N}^{+}+4e^{-}\end{array}\right\},n_{\mathrm{e}}\sim 4e^{-}$$

IV. Photoionization-Induced Precursor-Driven LSD Wave

The description of the 1-D LID (photoionization-induced laser discharge) model is as shown in Fig. 4 and given in the following. The ultra-violet (UV) radiation (photon flux) from the plasma is absorbed by the ambient gas ahead of the shock front. This leads to the generation of seed electrons (precursor) in a process termed as photoionization, and occurs when the plasma $h\nu$ exceeds the ionization potential of the gas. The precursor acts as an absorption medium ahead of the shock wave during the LSD regime and thus is accelerated by the inverse bremsstrahlung (IB) process resulting in avalanche ionization and subsequent rapid increase in n_{e}. The mechanism of electron-ion recombination tends to reduce n_{e} during this regime. The 1-D LID model describes the relation of the LSD wave velocity U, to the photon flux and the precursor ahead of the shock wave.

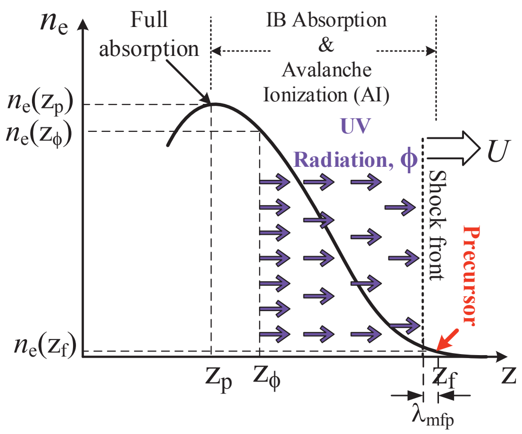

Figure 4. Description of the 1-D laser-induced discharge model.

The 1-D LID model uses the conservation equation of n_{e} as defined for the streamer head expansion in an electric field[10]. The equation is presented in Eq. (4) and the solution for the ionization front velocity U_{R} (, where R means with recombination effect) considering steady state condition, is given in Eq. (5). $n_{\mathrm{e}}(z_{\mathrm{f}})$ is obtained from the relation expressed by Eq. (6). Thus, U_{R} is obtained by solving Eqs. (5) and (6).

$$dn_{\mathrm{e}}/\mathrm{d}t=(\partial n_{\mathrm{e}}/\partial t)-U_{\mathrm{R}}(\partial n_{\mathrm{e}}/\partial z)=\nu_{\mathrm{eff}}n_{\mathrm{e}}. \tag{4}$$

$$U_{\mathrm{R}}=\frac{\nu_{\mathrm{eff}}|z_{\mathrm{f}}-z_{\mathrm{p}}|}{\ln\left(n_{\mathrm{e}}(z_{\mathrm{p}})/n_{\mathrm{e}}(z_{\mathrm{f}})\right)}. \tag{5}$$

$$n_{\mathrm{e}}(z_{\mathrm{f}})=\phi/U_{\mathrm{R}}. \tag{6}$$

Where ν_{eff} is the effective ionization frequency which takes into account the effect of electron-ion recombination, as shown in Eq. (7). α_{R}, which is a function of electron temperature is the total recombination rate coefficient, and was obtained from the NIFS-DATA 54 (June 1999) Research Report[15].

$$\nu_{\mathrm{eff}}=\nu_i-\alpha_{\mathrm{R}}n_{\mathrm{e}}. \tag{7}$$

The total recombination is the sum of the radiative and dielectric recombination processes[15]. The reaction equations showing these processes are as presented below.

$$\begin{array}{rl}\mathrm{Ar}^{+}+e^{-}\rightarrow\mathrm{Ar}+h\nu & \text{(radiative)}\\ \mathrm{Ar}^{+}+e^{-}\Rightarrow\ \mathrm{Ar}^{**}\rightarrow\mathrm{Ar}+h\nu & \text{(dielectric)}\\ \mathrm{N}^{+}+e^{-}\rightarrow\mathrm{N}+h\nu & \text{(radiative)}\\ \mathrm{N}^{+}+e^{-}\Rightarrow\ \mathrm{N}^{**}\rightarrow\mathrm{N}+h\nu & \text{(dielectric)}\end{array}$$

Considering a simple 1-D case and assuming that half of the total plasma radiation goes in both directions along the distance z, the photon flux of the UV radiation from the plasma, ϕ was estimated using Eq. (8).

$$\phi = 2\pi \int_{\nu_{\rm eff}}^{\infty} \int_{0}^{5\lambda_{\rm mfp}} \frac{i_\nu \exp\left(-z/\lambda_{\rm mfp}\right)}{h\nu_{\rm eff}} dz d\nu \ . \qquad (8)$$

Here i_ν and $\lambda_{\rm mfp}$ are the radiation due to the free-free and the free-bound transitions, and the mean free path of photon-absorption respectively. i_ν which is a function of particle number density and temperature is given by the sum of the free-free and the free-bound transitions of radiation[16,17]. Using the experimentally obtained peak $n_{\rm e}$ and maximum $T_{\rm ex}$, i_ν was estimated. In Fig. 4, $z_{\rm f}$ is the position of first avalanche ionization due to the energy absorption mechanism of the precursor. The distance between z_ϕ and $z_{\rm f}$ defines the integrated $n_{\rm e}$ contributing to ϕ (total number of photons per unit area per second) at $z_{\rm f}$.

V. Results and Discussion

Table 1 shows the comparison of measured and estimated parameters at an elapsed time of 1.4 µs. Heat deposited in both gases, q are quantitatively similar as shown, however $T_{\rm ex}$ in N_2 is higher ($T_{{\rm ex,N}_2} \cong 2T_{\rm ex,Ar}$). This experimental observation is explainable per the assumption that the heat absorbed in N_2 is used for plasma heating; whiles in Ar, it is used for plasma displacement. Thus per the 1-D LID model, N_2 would have a higher radiative energy and a higher rate of seed electron generation.

TABLE 1. Measured and estimated parameters at 1.4 µs.

Parameters	Argon	Nitrogen
Peak $n_{\rm e}$, $10^{24}{\rm m}^{-3}$	3.23 ± 0.14	3.16 ±0.27
$T_{\rm ex,max}$, eV	2.44 ± 0.13	4.13 ± 0.13
Measured $z_{\rm p}$, 10^{-4} m	8.5	7.0
Estimated $n_e(z_{\rm f})$, 10^{22} m^{-3}	0.13	1.14
$\alpha_{\rm R}$, m^{3}s^{-1}	2.5×10^{-18}	2.5×10^{-18}
Estimated ϕ, 10^{24} m^{-2}s^{-1}	1.96	17.3
Measured U, kms^{-1}	1.04	1.03
Estimated U, kms^{-1}	1.50	1.52
Estimated $U_{\rm R}$, kms^{-1}	1.17 ± 0.14	1.13 ± 0.26
Measured q, MJkg^{-1}	1.30	1.11
Measured z, mm	4.25	3.36

Figure 5 shows the plots of estimated velocities with and without recombination effect (obtained from the 1-D LID model and measured parameters), and measured velocities respectively versus laser intensity per unit density. The measured ionization front velocities approached the Chapman-Jouguet (C-J) condition irrespective of the constituent ambient gas within the low intensity zone, but were characterized by a weak overdriven detonation in the high intensity zone. Thus during LSD termination, the ionization front velocity is defined by the C-J line.

The estimated U in both Ar and N_2 within the LSD termination region were similar and about 1.5 times greater than their respective measured U as shown in Table 1. More so, the estimated $U_{\rm R}$ in both Ar and N_2 were approximately equal in magnitude to their respective measured U. This observation clearly depicts the effect that recombination has on the LSD wave velocity. Table 2 explains the similarity in estimated velocities by showing the per unit (p.u) quantities of the parametric values of Eq. (5) and with Ar parameters as the base units.

TABLE 2. Per unit parameters with Ar as base unit.

Parameters	Argon	Nitrogen
ν_i	1.00	0.83
$\lvert z_{\rm f} - z_{\rm p} \rvert$	1.00	0.82
$1/\ln\left(n_{\rm e}(z_{\rm p})\right)$	1.00	1.00
$-1/\ln(n_{\rm e}(z_{\rm f}))$	1.00	0.96
Estimated U	1.00	1.02
Estimated $U_{\rm R}$	1.00	0.97

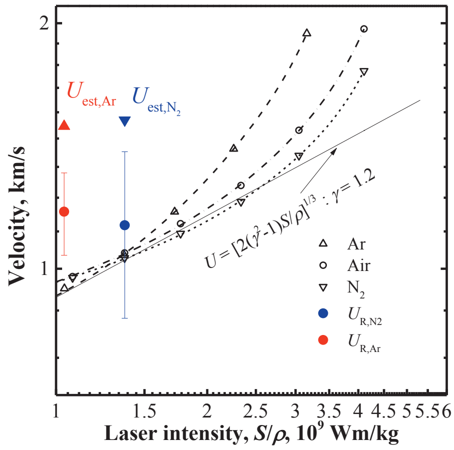

Figure 5. Measured and estimated ionization front velocities.

VI. Conclusion

The LSD wave propagation speed was estimated using a photoionization-induced laser discharge model similar to a streamer discharge model. In order to count UV photon flux toward the wavefront, n_e and T_{ex} were measured in a monoatomic gas, Ar and a diatomic gas, N_2 within the LSD termination region using the two-wavelength Mach-Zehnder interferometer and optical emission spectroscopy respectively.

Estimated wavefront velocities in Ar was almost the same as the one in N_2 regardless of the difference in first ionization energy by a photon and in electron bombardment ionization/ dissociation cross section in each gas. This is consistent with the observed LSD wave velocity tendency.

The 1-D LID model predicted the LSD wave velocity U_R as depicted in Table 1 and Fig. 5. Hence the LSD wave generation and propagation, is a photoionization-induced precursor-driven phenomenon and therefore independent of shock compression effects. The significance of the electron-ion recombination mechanism in the description of the 1-D LID model was observed in the prediction of U_R in both gases.

Acknowledgment

This work was supported by a Grant-in-Aid for Scientific Research (A), No. 15H02320, sponsored by the Ministry of Education, Culture, Sports, Science and Technology (MEXT), Japan.

References

[1]Frisbee, R. H., Horvath, J. C. and Sercel, J. C., "Laser Propulsion for the Orbital Transfer Mission," *AIAA Paper*, 85-1224 1985.

[2]Resendes, D. P., Mota, S., Mendonca, J. T., Sanders, B., Encarnacao, J., and Gonzalez del Amo, J., "Laser Propulsion for Ground Launch," *Journal of Propulsion and Power*, Vol. 23, No. 1, 2007, pp. 73-80.

[3]Kantrowitz, A., "Propulsion to Orbit by Ground-Based Lasers," *Astronautics & Aeronautics*, Vol. 10 1972, pp. 74-76.

[4]Myrabo, L. N., Messitt, D. G., and Mead Jr., F. B., "Ground and Flight Tests of a Laser Propelled Vehicle," *AIAA Paper*, 98-1001, Reno 1998.

[5]Collins, P., "The promise of electricity from space for world economic development," *5th International Energy Conference Proceedings*, Vol. 3 1993, pp. 50–59.

[6]Mori, K., Komurasaki, K., and Arakawa, Y., "Influence of the focusing f number on the heating regime transition in laser absorption waves," *Journal of Applied Physics*, Vol. 92, No. 10 2002, pp. 5663-5667.

[7]Mori, K., Komurasaki, K., and Arakawa, Y., "Energy transfer from a laser pulse to a blast wave in reduced-pressure air atmospheres," *Journal of Applied Physics*, Vol. 95, No. 11 2004, pp. 5979-5983.

[8]Mori, K., Komurasaki, K., and Arakawa, Y., "Threshold laser power density for regime transition of a laser absorption wave in a reduced-density air atmosphere," *Applied Physics Letters*, Vol. 88, 121502 2006.

[9]Ushio, M., Komurasaki, K., Kawamura, K., and Arakawa, Y., "Effect of laser supported detonation wave confinement on termination conditions," *Shock Waves*, Vol. 18 2008, pp. 35-39.

[10]Raizer, Y. P., “Laser-Induced Discharge Phenomenon,” *Studies in Soviet Science*, Consultants Bureau, New York 1977, pp. 199-206.

[11]Shimamura, K., Hatai, K., Kawamura, K., Fukui, A., Fukuda, A., Wang, B., Yamaguchi, T., Komurasaki, K., and Arakawa, Y., “Internal structure of laser supported detonation waves by two-wavelength Mach-Zehnder interferometer,” *Journal of Applied Physics*, Vol. 109, 084910 2011.

[12]Raizer, Y. P., Sov. Phys. *JETP*, Vol. 21, No. 5 1965, pp. 1009-1017.

[13]Shimamura, K. Komurasaki, K., Ofosu, J. A., and Koizumi, H., “Precursor ionization and propagation velocity of a laser-absorption wave in 1.053 and 10.6 μm wavelengths laser radiation,” *IEEE Transactions on Plasma Science*, Vol. 42, No. 10, Oct. 2014, pp. 3121-3128.

[14]Tognoni, E., et al., “From sample to signal in LIBS: a complex route to quantitative analysis,” in *Laser-induced Breakdown Spectroscopy: Fundamentals and Applications*, edited by Miziolek, W. A., Palleschi, V., and Schechter, I., New York: Cambridge University Press, 2006, pp. 122-166.

[15]Kato, T. and Asano E., “Comparison of Recombination Rate Coefficients Given by Empirical Formulas for Ions from Hydrogen through Nickel,” *National Institute for Fusion Science,* NIFS-DATA-54, June 1999, pp. 14, 79.

[16]Bose, T. K., *High Temperature Gas Dynamics*, Springer, New York, 1979.

[17]Griem, H. R., *Principles of Plasma Spectroscopy*, Cambridge University Press, 1997.